Appl. Phys. B 69, 407–412 (1999) / Digital Object Identifier (DOI) 10.1007/s003409900163

Applied Physics B
Lasers
and Optics
© Springer-Verlag 1999

Atom lithography with a cold, metastable neon beam

P. Engels*, **S. Salewski, H. Levsen, K. Sengstock, W. Ertmer**

Institut für Quantenoptik, Universität Hannover, Welfengarten 1, 30167 Hannover, Germany
(Fax: +49-511/762-2211, E-mail: engels@iqo.uni-hannover.de)

Received: 29 June 1999/Revised version: 30 August 1999/Published online: 10 November 1999

Abstract. We study different aspects of atom lithography with metastable neon atoms. Proximity printing of stencil masks is used to test suitable resists that are sensitive to the internal energy of the atoms, including dodecanethiols on gold and octadecyltrichlorosilanes grown on a SiO_2 surface. As an example of patterning the atomic beam with laser light, we create parallel line structures on the surface with a periodicity of half the laser wavelength by locally de-exciting the atoms in a standing quenching wave.

PACS: 03.75.Be; 32.80.Lg; 42.82.Cr

The field of laser manipulation of the external degrees of freedom of neutral atoms has stimulated many areas in atomic physics, precision measurements, and quantum optics in recent years, and has opened up the new field of atom optics [1]. Various atom optical elements that manipulate atomic beams similar to the way lenses and mirrors manipulate light have successfully been demonstrated. The application of these atom optical elements for the creation of structures with sub-100-nm resolution defines the increasing field of atom lithography. The main potential of atom lithography arises from the ability to manipulate different elements selectively and in a parallel way. A particular example of an application is the creation of periodic three-dimensional doping structures by using a simultaneous deposition process of several different elements and manipulating each element in a different way. One possibility for the creation of nanostructures with neutral atoms is the direct deposition of the atoms on a surface [2–5]. Another, complementary method is to use the high internal energy in atomic metastable states [6–9] or the reactivity of Cs atoms [10, 11] to expose surfaces covered with suitable resists. These techniques seem to be especially well suited for studying the ultimate resolution limits of atom lithography because they avoid any feature broadening caused by the growth process of material on the substrate [12]. In the case of resist-based lithography, no additional broadening mechanisms have been reported so far, though they might be present.

In this paper we discuss several questions, problems, and regimes in connection with atom lithography with metastable atoms, as well as different resists and their sensitivity to Ne* exposure. In addition for the first time atom lithographic experiments with a laser-manipulated pure, cold, and slow atomic beam of Ne* are discussed. For this, a laser-decelerated beam of Ne* in the $3s[3/2]_2$ state is selectively spatially deflected from the beam region so that no ions, UV-photons or atoms in other metastable states are present in the deflected beam. This will allow for very clean exposure processes. The setup uses a slow atomic beam with a mean velocity as low as 26 m/s for atom lithography. Since even at thermal velocities the kinetic energy of the atoms is only on the order of a few meV whereas the internal energy of the metastable Ne* amounts to 16.6 eV, the low velocity of our beam does not substantially change the resist damaging process. However, it allows us to study atom optical regimes that are complementary to those of previously existing experiments. In addition, a completely oil-free vacuum chamber is used for the exposure process, so that no contamination with long carbon chain molecules can change the atom lithographic process during exposure as observed in other experiments. In order to achieve highest resolution, the choice of suitable resists is important. Therefore special care was taken in this paper to check existing resists for their sensitivity to Ne* and to test new or partially new resist techniques.

1 Experimental setup

In order to achieve feasible exposure times, a setup used for atom lithography with metastable rare gas atoms has to be designed for a high flux. Typically the rare gas atoms are excited to a metastable state in a gas discharge source. Since the excitation process is very inefficient (on the order of 10^{-5}), typical beam sources are limited to a brightness on the order of 10^{14} atoms/sr s. However laser-cooling techniques are well suited to collimate and compress the metastable beam, increasing the flux density by several orders of magnitude [13, 14]. A schematic overview of our experimental setup is shown in Fig. 1. We use a liquid-nitrogen-cooled

* Corresponding author.

dc gas discharge source to excite the neon atoms. The first metastable state, $3s[3/2]_2$, has a lifetime of approximately 22 s [15]. The closed transition to the $3p[5/2]_3$ state is used for laser cooling. Behind the discharge region the beam is collimated in a transverse Doppler cooling zone. It then passes through a skimmer and is decelerated in a Zeeman slower to a velocity of about 70 m/s. The Zeeman slowing is done in order to prepare the atoms for a subsequent two-dimensional magneto-optical molasses (2D-MOM). In this 2D-MOM a magnetic quadrupole field, with a gradient increasing along the axis of the molasses from 65 G/cm to 350 G/cm, together with two pairs of σ^+–σ^- polarized laser beams is used for transverse cooling, compression, and deflection of the atomic beam [16, 17]. The use of specially shaped permanent magnets allows for a very compact design of the 2D-MOM. The atoms are guided along the axis of the quadrupole field so that a deflection of the atomic beam can be achieved by tilting the axis of the molasses relative to the axis of the Zeeman slower. In our setup the deflection angle is 68°. As mentioned above, the deflection is used to remove any unwanted particles from the atomic beam. Besides, it results in a further reduction of the atomic longitudinal velocity down to 26 m/s. The longitudinal velocity spread of this beam is 6 m/s (rms value) (for the results discussed below, this was the relevant width) but can be reduced to 1.3 m/s (rms value) with the help of an additional running optical molasses that crosses the atomic beam under an angle of 15° (see Fig. 1) [16]. A low longitudinal velocity spread is important e.g. for reducing chromatic effects in experiments that aim at writing small features by focusing the atomic beam with dipole forces in detuned standing laser waves. The detuning and the alignment of the laser beams that are used for the 2D-MOM can be optimized either for maximum flux or for low transverse momenta. A typical value for the atomic flux is approximately 6×10^8 atoms/s through a beam diameter of 70 μm. The minimum transverse rms velocities achieved with this setup are 6 cm/s, which is close to twice the recoil limit of $v_{\mathrm{rec}} = 3.1$ cm/s. The beam brightness is typically 1.5×10^{14} atoms/sr s.

A detector consisting of a chevron-type multi-channel plate (MCP), a phosphor screen, and an ICCD camera is monitoring the metastable beam. Metastable atoms hitting the MCP undergo a Penning ionization process and thereby release an electron. The flux of electrons is amplified by the MCP and generates fluorescence of a phosphor screen which is detected by the camera. The detector is positioned at a distance about 32 cm downstream from the two-dimensional beam-compression zone. Since the exit of the compression zone can be thought of as an almost pointlike source of atoms, the pictures taken with this detector are direct images of the transverse momentum distribution of the metastable atoms. The transverse momentum resolution of our detection system is better than 0.5 recoil momenta in this configuration. As will be explained below, this detector not only allows for an immediate determination of the flux and the transverse momentum profile, but also proves to be a very useful tool for aligning the light fields used for patterning relative to the atomic beam.

The light for the laser-cooling stages is produced by a dye laser at 640.2 nm which is directly frequency locked on the atomic beam by fluorescence spectroscopy. For patterning the atomic beam with light forces in standing waves, we use a master-slave diode laser system at 640.2 nm or 633.6 nm. The master is grating-stabilized in an external cavity configuration. It is locked to a neon dc-discharge cell, and its frequency can be shifted by an AOM. The light is transferred to the vacuum chamber with a single-mode optical fiber. A standing wave is formed by a back-reflection mirror inside the vacuum chamber.

2 Patterning the beam with light forces

Various methods for patterning the atomic beam in a lithographic experiment are possible. For the creation of periodic line structures the dipole force in a blue-detuned standing wave in front of the substrate can function as a "grin lens array" for the atoms [2]. Alternatively we employ a standing quenching wave in front of the substrate, as first demonstrated in the experiment described in [18].

Quenching means in our case that metastable Ne* atoms are optically excited from the $3s[3/2]_2$ state to the $3p[5/2]_2$ state from which they decay into the atomic ground state with a probability of about 60% (whereas with a probability of 40% they decay back into the metastable state). The atoms release their internal energy in form of a UV photon and therefore become ineffective for the subsequent patterning process. If the parameters of the quenching wave are chosen in such a way that all the atoms traveling through the antinodes are quenched whereas atoms traveling close to the nodes

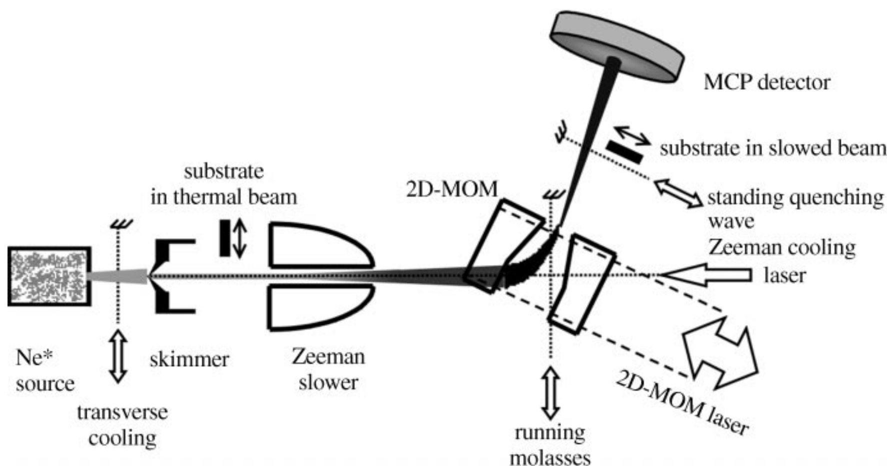

Fig. 1. Schematic diagram of the experimental setup

remain in the metastable state, the standing quenching wave is a "virtual slit array" for the atoms [19].

In order to compensate for diffraction effects that are connected with the localization of the metastable atoms in the regions near the nodes, the standing wave is detuned to higher frequencies so that a dipole potential is created that pushes the atoms into the nodes. In a quantum mechanical picture, the blue-detuned quenching wave creates a dipole potential and, depending on the exact experimental parameters, a small number of eigenstates is occupied by the atoms when entering the standing wave region. In a harmonic approximation of the potential near each node, the different eigenstates have a quenching rate proportional to $2n+1$, where n denotes the harmonic oscillator level. This reflects the different overlap of the eigenstates with the quenching light. To achieve smallest feature widths in a lithographic experiment using standing wave quenching, the experimental parameters are chosen in such a way that mainly the harmonic oscillator ground state is left in the beam whereas all higher eigenstates are quenched to a large degree.

We have performed several series of measurements studying the quenching process for atom lithographic applications. Besides the spatial confinement of atoms in a standing quenching wave, we have also studied the substantial narrowing of the transverse momentum distribution δp of atoms transmitted through standing quenching waves. Figure 2 shows momentum distributions of our atomic beam without and with a quenching laser beam. The localization of the atoms near the nodes within the standing wave first leads to a spread of the transverse momentum distribution δp, but as the atoms exit the wave adiabatically, an adiabatic compression of δp takes place [20]. In the case of Fig. 2 the momentum width of the transmitted ensemble (2b) is 1.3 $\hbar$k (rms) whereas the width of the atomic beam (2a) is 4.7 $\hbar$k (rms).

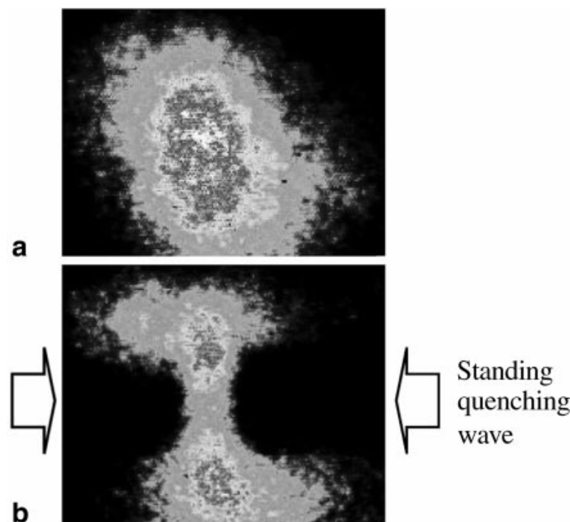

Fig. 2a,b. Cross section of the velocity distribution of the atomic beam taken with the MCP detector. **a** Atomic beam profile without quenching laser. **b** Atomic beam profile with a weak, horizontal, blue-detuned quenching laser beam. In order to demonstrate the effect, the waist of the quenching beam was chosen smaller than the waist of the atomic beam in this picture. Before the exposure of a sample in a lithographic experiment, the position of the transmission zone within the atomic beam profile is used for the alignment of the standing quenching wave orthogonal to the atomic beam

A detailed analysis of our experimental data concerning this particular aspect in comparison to a numerical simulation will be published elsewhere. This momentum compression can be used as a first step in a two-step focusing geometry in order to reduce the momentum spread so that spherical aberrations are lessened.

For a successful patterning of samples with beams shaped by light forces, the precise alignment of the sample, the standing wave, and the atomic beam relative to each other is essential. To ensure that the sample is orthogonal to the back-reflection mirror and therefore parallel to the standing wave, it is clamped to a right-angle prism which is directly attached to the back-reflection mirror. The mirror is held by a motorized mount so that the sample can be tilted and moved in and out of the atomic beam. Before each exposure the sample is moved out of the atomic beam, and the standing wave is aligned orthogonal to the atomic beam. For this, the transverse momentum spread of the atomic beam after passing through the standing quenching wave is monitored on the MCP detection system as described above for different tilting angles of the standing wave relative to the atomic beam. The standing quenching wave leads to a narrowing of the transverse momentum spread, and it is properly aligned relative to the atomic beam when the center of the quenching zone coincides with the center of the unquenched beam (Fig. 2b).

Evidence for the selective transmission of atoms through the nodes of the standing quenching wave can be gained from a comparison of the number of metastable atoms transmitted by the standing wave relative to the number of atoms transmitted by a traveling wave of the same ingoing laser power. One example for such a transmission rate as a function of laser power is shown in Fig. 3 for a laser detuning of +100 MHz and a waist of 100 μm. Whereas at low intensities the transmission through a traveling wave is higher than the transmission through the standing wave, the situation is reversed at higher laser powers. This can be explained as follows: at low laser powers, only a small fraction of the atoms is quenched, and the quenching in the standing wave is

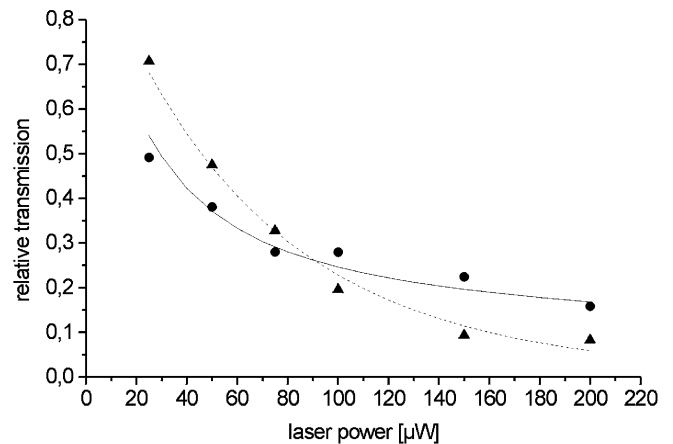

Fig. 3. Transmission of atoms in the metastable state through a standing quenching wave and a traveling quenching wave as a function of laser power. In both cases the detuning of the quenching wave was +100 MHz, and the waist was 100 μm. The graph shows the measured values for the standing wave (*points*) and the traveling wave (*triangles*). The lines depict theoretical values for the case of the standing wave (*solid line*) and the traveling wave (*dotted line*) and have been calculated by the model described in the text

stronger because the standing wave contains twice the power (standing and traveling waves with the same ingoing laser power are compared). At higher intensities, in the traveling wave quenching tends to saturation and nearly all atoms are quenched. In the standing wave atoms may travel through the nodes, leading to a higher transmission rate of the metastable state.

To substantiate this explanation, the lines in Fig. 3 show the result of a simple model calculation. For this, it is assumed that the atoms move through the quenching wave with constant longitudinal velocity (x direction). The transmission is then given by

$$T = \exp\left[-\int \Lambda \frac{\Gamma}{2} \frac{S(x)}{1+S(x)+\frac{4\Delta^2}{\Gamma^2}} \frac{1}{v}\,\mathrm{d}x\right], \quad (1)$$

where v denotes the velocity of the atoms, and Δ is the detuning of the laser relative to the quenching transition. Γ denotes the natural line width of the transition and the integral is calculated along the trajectory of the atoms. $S(x) = I(x)/I_{\text{sat}}$, the ratio of the laser intensity divided by the saturation intensity, denotes the spatially varying saturation parameter and depends on the laser waist, power, and the geometry (standing wave or traveling wave). The fact that only 60% of the excited atoms actually decay into the ground state is accounted for by including the branching ratio $\Lambda = 0.6$ of this transition. In the case of the standing quenching wave, the transmission is in addition averaged over one period of the standing wave. This simple model does not contain any fit parameters and, as shown in Fig. 3, describes the measurements well. Such measurements provide us with insight into the patterning process before exposing samples. The results of the localization within a standing quenching wave in combination with resists will be discussed in the following section.

3 Resists

Atom lithography with metastable rare gas atoms requires resists that are sensitive to the internal energy of the atoms. In the case of metastable neon, the internal energy is 16.6 eV, which is much larger than typical chemical bond energies. Because of the low kinetic energy in the atomic beam the atoms do not penetrate into the samples and release their internal energy as soon as they touch the surface. Therefore ultrathin resists can be used.

One example that has been used in atom lithographic experiments is a self-assembled monolayer (SAM) of alkanethiols on a gold-coated silicon wafer [6, 7, 9]. The molecules form a highly ordered monolayer which makes the surface hydrophobic and protects it against aqueous chemical etching solutions. When the sample is exposed to the metastable rare gas atoms, the SAM is damaged and the underlying gold layer can be etched away. In a second etching step this patterned gold layer can then be used as a mask for etching into the silicon. Since the gold-etching step is isotropic, very thin gold layers are used. Typical values are 20 nm–30 nm thickness of gold on top of an up to 10 nm thin Cr buffer layer. We usually prepare the SAM resist by immersing samples with clean gold surfaces into a 1 mM solution of thiols, for example dodecanethiols, in ethanol for 10–24 h. Previously the dosages required to sufficiently damage a SAM layer of dodecanethiols on gold were known only for exposure to Ar* and He* [7, 9, 21]. It was found that even though the internal energy of He* is only twice as high as the internal energy of Ar*, the exposure times for Ar* are approximately ten times longer than for He*. This may hint at different resist damaging mechanisms involved in the case of the two elements.

We have exposed samples of SAM resists for different times and at different beam intensities. To measure the contrast a simple grid in front of the sample was used as a mask for the atomic beam. Figure 4 shows a typical example. This sample was exposed to a dosage of about 9 Ne* atoms per SAM molecule in the thermal Ne* beam with mean velocities of 850 m/s. HV deflection plates were used to remove any ions in the beam. This measurement configuration is comparable to the ones that were used by other groups for the determination of the values for Ar* and He*. After the exposure, the gold layer in the areas that were not shaded by the mask was etched in a solution consisting of 1 M KOH, 0.1 M $K_2S_2O_3$, 0.01 M $K_3Fe(CN)_6$, and 0.001 M $K_4Fe(CN)_6$ [22]. From these measurements we found that 5–10 Ne* atoms per SAM molecule, which means exposure times of 2–4 min in a typical thermal beam, are sufficient to produce a nearly perfect contrast. This is a dosage intermediate between the dosages of He* and Ar*. However, since the values for example for He* found by different experiments vary substantially, we plan a direct comparison of Ne* with He* and Ar* within our setup to avoid problems associated with different experimental conditions.

As explained above the etched gold layer can serve as a mask for wet-chemical etching into the silicon. We typically

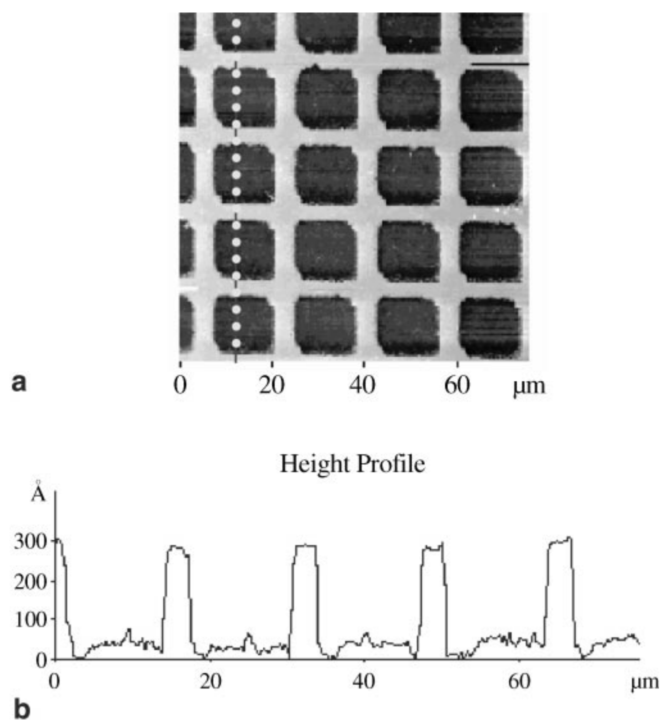

Fig. 4a,b. Proximity printing of a 1500-mesh gold mask using a SAM layer of dodecanethiols on gold as resist. The sample was exposed in the thermal beam with a dosage of about 9 Ne* per SAM molecule and is shown after the gold etching step described in the text. **a** AFM image. **b** Line analysis of the line marked in Fig. 4a

use a KOH solution for this process. Another technique for transferring the pattern into the underlying Si substrate has been demonstrated by Lu et al. [9] who used plasma etching and achieved depths of 580 nm and a side-wall inclination of better than 86°. The finite thickness of the gold films that is needed because of the growth properties of the gold ultimately limits the resolution of the technique to few tens of nm.

An alternative SAM resist that circumvents the resolution limits given by the gold surface is a polysiloxane layer, in particular octadecyltrichlorosilane (OTS), directly on a SiO_2 surface [23]. In our lab we prepare OTS SAMs by immersing the Si wafer samples into a 1 vol % OTS solution in bicyclohexyl for approximately 2 h, after preparing them in several cleaning steps and a 20-min dip in Piranha solution (a 30 : 70 v/v mixture of 30% H_2O_2 and 96% H_2SO_4 at 80 °C). During the immersion the solution is kept in a nitrogen atmosphere. For the OTS samples we typically use exposure times that are more than four times longer than for thiols on gold. In order to demonstrate that the local damage is 'visible' on the sample, Fig. 5a shows the local change of hydrophobicity of the surface after a 10 min exposure to a thermal beam of Ne* atoms through a 2000 mesh gold mask. Figure 5a is a light microscopy image of the probe after a short exposure to humidity. In a two-step wet-chemical etching procedure, involving a short HF dip and a successive KOH dip, we were able to transfer the features into the silicon substrate. The AFM image Fig. 5b shows the result of this etching procedure, and Fig. 5c is a line analysis after averaging over the small region marked in Fig. 5b. So far, feature depths up to 20 nm were achieved, but further refinements of the etching procedures will be performed in order to reduce the surface roughness. Alternatively to the wet-chemical etching, the different wetting properties of the exposed vs. unexposed areas could possibly also be exploited for a selective deposition of another thin polymer film on top of the OTS layer.

Instead of using surfaces that are precoated with a resist layer, the deposition of background molecules during the exposure can also be employed. In many setups that use diffusion pumps connected to the experimental chambers, pump oil molecules are present as a background vapor, so this technique has been termed contamination lithography. Pump oil molecules that physisorb on the surface are cracked by the incident metastable atoms, leading to the formation of a carbonaceous resist. This effect is well known from e-beam lithography where it was used already more than 30 years ago (see, for example, [24]). In our setup only the source chamber is pumped by a diffusion pump. It is separated from the experimental chamber by a skimmer, a differential pumping stage, and the Zeeman slower tube. The vacuum pressure in the experimental chamber is better than 2×10^{-7} mbar. Therefore we have no uncontrolled contamination lithography. In addition we have checked this by exposing silicon samples for much longer than any other typical exposure time, without seeing any contamination lithography contrast.

For a demonstration of the effect of contamination lithography, a sample was placed behind a 2 mm skimmer in the source chamber where diffusion pump oil is still present. A 2000 mesh gold grid was directly attached to a piece of silicon wafer that had been prepared by a short HF dip. After a 4 h exposure the formation of an etch resist film with a thickness of less than 1 nm in the exposed areas could be observed by tapping mode AFM. In a wet-chemical etching step using an aqueous ammonium hydroxide solution the pattern was then transferred into the silicon. In this demonstration an etching depth of 800 nm was achieved with no detected roughening or pits in the exposed areas (Fig. 6), showing that contamination lithography with Ne* is capable of providing very good contrast, though at the cost of long exposure times.

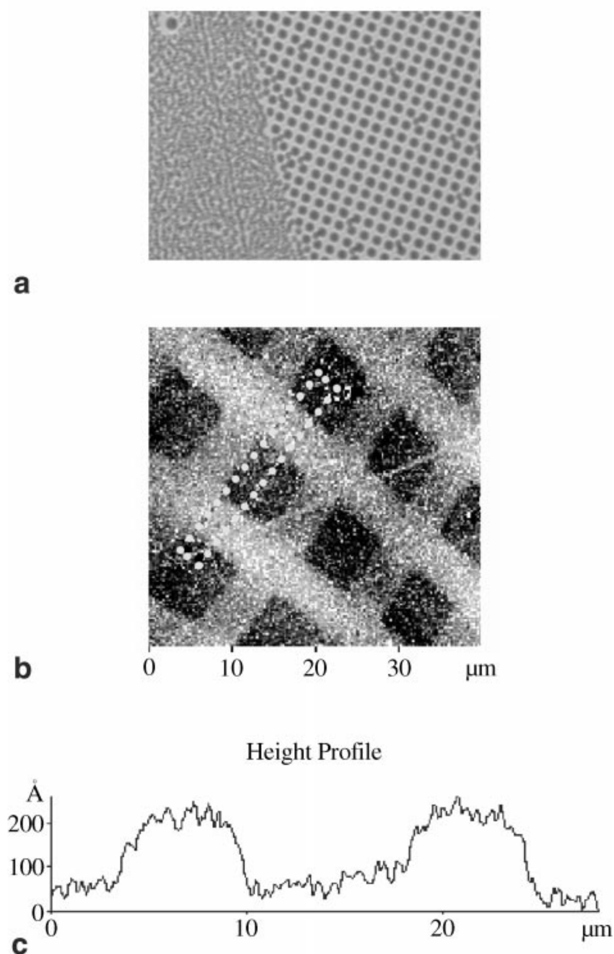

Fig. 5. a Change of the wettability of an OTS layer after proximity printing of a 2000-mesh gold mask for 10 min in the thermal beam. The left part of the picture shows an unexposed area that had been covered by the rim of the mask. Light microscopy image. **b** AFM image of the pattern after etching into the Si substrate. **c** Line analysis after integration over the region marked in Fig. 5b

As a preliminary result for atom lithography with slow, cold metastable Ne* atoms, Fig. 7 shows line structures, where atoms were localized in a 1-dimensional blue-detuned standing quenching wave. The light field had a waist of 100 μm, a detuning of about 1 GHz, and a power of 600 μW. The sample used in this measurement was a SAM-coated gold layer as discussed above. For the exposure the standing wave was slightly clipped by the sample so that the distribution of the atoms inside the standing wave is observed. An integral line analysis (Fig. 7b) over the region marked in Fig. 7a reveals that the periodicity of the lines is given by half the wavelength of the standing wave. Since this wavelength can be determined to a very high precision, atom lithographic line

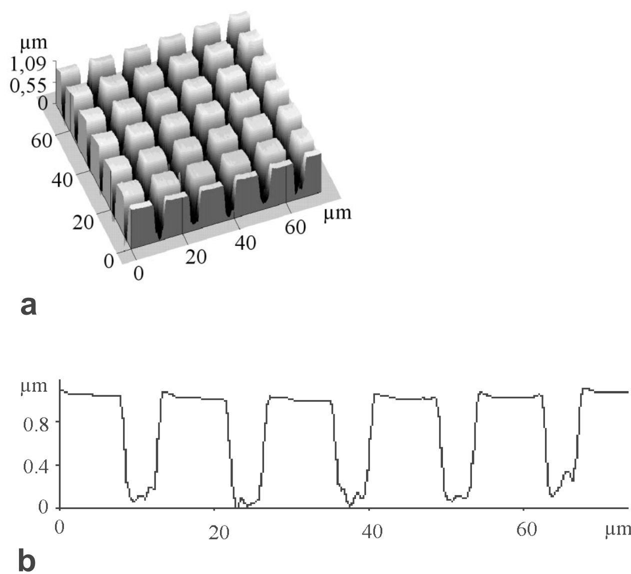

Fig. 6a,b. Demonstration of the etch resistance achieved with a contamination layer after a 4 h exposure of Si in the thermal beam. **a** 3D rendering of an AFM image. **b** Line analysis

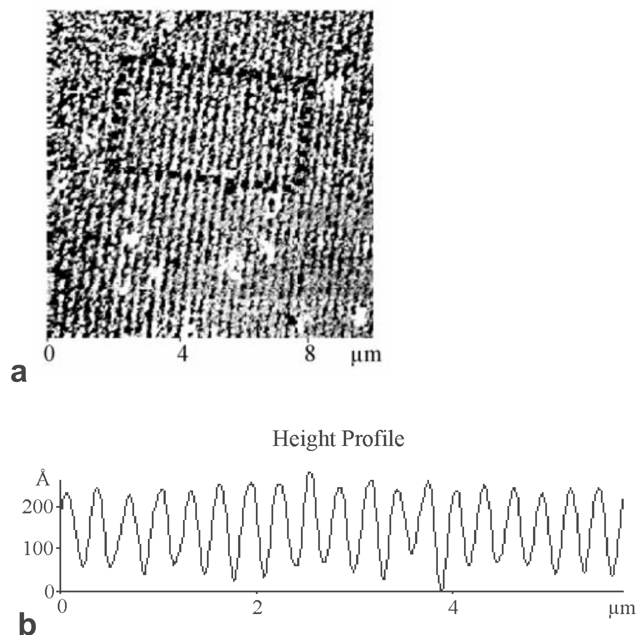

Fig. 7a,b. Line structures created with the deflected atomic beam by localizing the atoms in a blue-detuned quenching beam. **a** AFM image. **b** Line analysis after integrating over the region marked in Fig. 7a. The periodicity of the lines is given by half the wavelength of the light used for the quenching and focusing

structures are interesting objects for metrological purposes, for example length standards for AFMs [25].

4 Outlook

In the near future we will study the dependence of the line widths generated on various surfaces at different parameters when using focusing and quenching of atoms in standing waves. The running optical molasses in our setup allows us in addition to gain precise control over the longitudinal velocity spread of the atomic beam, whereas the use of an additional standing quenching wave allows us to manipulate the transverse momentum spread of the beam. Thus it will be possible to study the aberrations of atom optical lens systems and to determine the factors that ultimately limit the resolution of atom lithography.

Acknowledgements. This work was supported by the TMR-network "Nanofab". We would like to acknowledge discussions with Dr. Niesen, MPI Stuttgart, concerning sample preparation.

References

1. For a review article, see C.S. Adams, M. Sigel, J. Mlynek: Phys. Rep. **240**, 143 (1994)
2. G. Timp, R.E. Behringer, D.M. Tennant, J.E. Cunningham, M. Prentiss, K.K. Berggren: Phys. Rev. Lett. **69**, 1636 (1992)
3. J.J. McClelland, R.E. Scholten, E.C. Palm, R.J. Celotta: Science **262**, 877 (1993)
4. R.W. McGowan, D.M. Giltner, S.A. Lee: Opt. Lett. **20**, 2535 (1995)
5. U. Drodofsky, J. Stuhler, B. Brezger, Th. Schulze, M. Drewsen, T. Pfau, J. Mlynek: Microelectron. Eng. **35**, 285 (1997)
6. K.K. Berggren, A. Bard, J.L. Wilbur, J.D. Gillaspy, A.G. Helg, J.J. McClelland, S.L. Rolston, W.D. Phillips, M. Prentiss, G.M. Whitesides: Science **269**, 1255 (1995)
7. S. Nowak, T. Pfau, J. Mlynek: Appl. Phys. B **63**, 203 (1996)
8. S.J. Rehse, A.D. Glueck, S.A. Lee, A.B. Goulakov, C.S. Menoni, D.C. Ralph, K.S. Johnson, M. Prentiss: Appl. Phys. Lett. **71**(10), 1427 (1997)
9. W. Lu, K.G.H. Baldwin, M.D. Hoogerland, S.J. Buckman, T.J. Senden, T.E. Sheridan, R.W. Boswell: J. Vac. Sci. Technol. B **16**(6), 3846 (1998)
10. M. Kreis, F. Lison, D. Haubrich, D. Meschede, S. Nowak, T. Pfau, J. Mlynek: Appl. Phys. B **63**, 649 (1996)
11. K.K. Berggren, R. Younkin, E. Cheung, M. Prentiss, A.J. Black, G.M. Whitesides, D.C. Ralph, C.T. Black, M. Tinkham: Adv. Mater. **9**, 52 (1997)
12. W.R. Anderson, C.C. Bradley, J.J. McClelland, R.J. Celotta: Phys. Rev. A **59**(3), 2476 (1999)
13. J. Nellessen, J. Werner, W. Ertmer: Opt. Commun. **78**, 300 (1990)
14. M.D. Hoogerland, J.P.J. Driessen, E.J.D. Vredenbregt, H.J.L. Megens, M.P. Schuwer, H.C.W. Beijerinck, K.A.H. van Leeuwen: Appl. Phys. B **62**, 323 (1996)
15. F. Shimizu, K. Shimizu, H. Takuma: *Laser Spectroscopy IX* (Academic Press, New York 1989)
16. A. Scholz, M. Christ, D. Doll, J. Ludwig, W. Ertmer: Opt. Commun. **111**, 155 (1994)
17. M. Schiffer, M. Christ, G. Wokurka, W. Ertmer: Opt. Commun. **134**, 423 (1997)
18. K.S. Johnson, J.H. Thywissen, N.H. Dekker, K.K. Berggren, A.P. Chu, R. Younkin, M. Prentiss: Science **280**, 1583 (1998)
19. A.P. Chu, K.K. Berggren, K.S. Johnson, M.G. Prentiss: Quantum Semiclass. Opt. **8**, 521 (1996)
20. A.P. Chu, K.S. Johnson, M.G. Prentiss: Opt. Commun. **134**, 105 (1997), and references therein
21. A. Bard, K.K. Berggren, J.L. Willbur, J.D. Gillaspy, S.L. Rolston, J.J. McClelland, W.D. Philips, M. Prentiss, G.M. Whitesides: J. Vac. Sci. Technol. B **15**(5), 1805 (1997)
22. Y. Xia, X. Zhao, E. Kim, G.M. Whitesides: Chem. Mater. **7**, 2332 (1995)
23. S.B. Hill, C.A. Haich, F.B. Dunning, G.K. Walters, J.J. McClelland, R.J. Celotta, H.G. Craighead, J. Han, D.M. Tanenbaum: J. Vac. Sci. Technol. B **17**(3), 1087 (1999)
24. A.N. Broers: In *Proceedings of the First International Conference on Electron and Ion Beam Science and Technology*, ed. by R. Bakish, (Wiley, New York 1964) p. 191
25. J.H. Thywissen, K.S. Johnson, N.H. Dekker, A.P. Chu, M. Prentiss: J. Vac. Sci. Technol. B **16**(6), 3841 (1998)